Current Optics and Photonics
Vol. 1, No. 3, June 2017, pp. 196-202

ISSN: 2508-7266(Print) / ISSN: 2508-7274(Online)
DOI: https://doi.org/10.3807/COPP.2017.1.3.196

An Automatic Corona-discharge Detection System for Railways Based on Solar-blind Ultraviolet Detection

Jiaqi Li*, Yue Zhou, Xiangyu Yi, Mingchao Zhang, Xue Chen, Muhan Cui, and Feng Yan

State Key Laboratory of Applied Optics, Changchun Institute of Optics, Fine Mechanics and Physics, Chinese Academy of Sciences, Changchun, Jilin 130033, China,

(Received February 28, 2017 : revised April 10, 2017 : accepted April 11, 2017)

Corona discharge is always a sign of failure processes of high-voltage electrical apparatus, including those utilized in electric railway systems. Solar-blind ultraviolet (UV) cameras are effective tools for corona inspection. In this work, we present an automatic railway corona-discharge detection system based on solar-blind ultraviolet detection. The UV camera, mounted on top of a train, inspects the electrical apparatus, including transmission lines and insulators, along the railway during fast cruising of the train. An algorithm based on the Hough transform is proposed for distinguishing the emitting objects (corona discharge) from the noise. The detection system can report the suspected corona discharge in real time during fast cruises. An experiment was carried out during a routine inspection of railway apparatus in Xinjiang Province, China. Several corona-discharge points were found along the railway. The false-alarm rate was controlled to less than one time per hour during this inspection.

Keywords : Corona inspection, Solar blind ultraviolet detection, Railway, Hough transform, Target recognition
OCIS codes : (040.5160) Photodetectors; (040.6040) Silicon; (060.0060) Fiber optics and optical communications; (060.4510) Optical communication

I. INTRODUCTION

Corona is often a sign of a defect, contamination, or malfunction of high-voltage electrical apparatus, such as electrical transmission lines, transformer insulators and bushings, and high-voltage supplies. Potential failure of electrical apparatus can be addressed though observing the occurrence of corona discharge [1, 2]. Electric locomotives, especially for high-speed railways, are being developed rapidly worldwide. While railways are getting longer and faster, their tolerance of faults gets smaller, since an accident might cause disruption of the railway or great economic loss. The electric locomotives engage a large amount of high-voltage electrical apparatus along the railway, much of which is under lightly contaminated or seriously contaminated conditions, such as inside tunnels or near deserts and other harsh environments. Corona and arcing discharge caused by environment contaminations and the aging of the equipment itself could be a threat to the safety of trains. Thus it is meaningful to detect the corona and arcing discharges along railways, as a preparation to eliminating these threats.

A number of methods have been applied to corona-discharge detection, including detection with ultraviolet (UV) cameras, infrared thermography and acoustic-emission detection [3]. Among these methods, specially designed ultraviolet cameras those detect corona discharges by monitoring the weak ultraviolet radiation (in the spectral range of 230-405 nm) emitted from a corona discharge in the air draw increasing attention. UV cameras working in the 240-280 nm region, which is usually called the UV solar-blind band, are able to acquire high-contrast images of corona discharge, due to the absence of background radiation (mainly solar irradiation) [4, 5]. Cameras of this type are able to detect extremely weak corona discharges emitting only a few photons. In recent years, solar-blind

*Corresponding author: lijiaqi@ciomp.ac.cn

Color versions of one or more of the figures in this paper are available online.

ultraviolet cameras have been utilized widely for corona inspection [6, 7].

Automatic recognition of the UV emitters during cruising is meaningful for a reducing inspection workload, especially for long-distance inspections. The simplest method is to report every event in which UV radiation is detected by the system. However, there is always some background noise in solar-blind UV detectors, including dark current and leakage photons [8], which would result in false alarms. The leakage photons might come from solar irradiance in the daytime, or from other irradiation such as lamps or fire. In high-SNR (signal to noise ratio) situations, noise can be removed easily by applying an appropriate threshold, but in corona-discharge inspections the intensity of ultraviolet radiation from a corona is always not much higher than that of the background noise, leading to some difficulties in distinguishing UV emitters from noise. Therefore, a specially designed target-recognition algorithm is necessary for automatic recognition of UV emitters (corona discharge).

In this paper, an algorithm based on a modified Hough transform [9, 10] is introduced for the recognition of corona discharges, which is an extension of Hough-transform applications towards the area of solar-blind ultraviolet imaging techniques. The Hough transform has been reported to be a robust and effective technique for target tracking, which has been intensively used for target observation by surveillance radar and infrared imaging [11-13]. In this work, a simple two-dimensional Hough transform is used to detect moving targets. The main challenge of the detection is controlling the probability of false alarm, as described in the following sections. To reduce the false-alarm rate, limitation methods in space and time domains are introduced into the algorithm. The limitation methods, which will be discussed in detail, prove to be significant in reducing the false-alarm rate during detection.

II. SCHEMATIC SETUP

The corona-discharge detection system includes a solar-blind UV camera and a visible camera, as shown in Fig. 1. The UV camera (Cam 1) consists of a solar-blind ultraviolet intensified charge-coupled device (ICCD), a specially designed solar-blind optical filter, and a UV objective lens. The ICCD (Proxitronic type HL4-V-ASB) consists of a solar-blind photocathode and an image intensifier coupled to a CCD. The UV filter and the objective lens were manufactured in our institute. The visible camera (Cam 2) consists of a standard CCD camera and an objective lens. Both cameras have 6.25° × 5° (H × V) field of view. The optical window of the system (L1) has high transmission in both ultraviolet and visible spectral ranges. L2 is a dichroic beam splitter. UV light passes through the beam splitter into the UV camera, while visible light is reflected from L2 and L3 and then directed into the visible camera. The two mirrors L2 and L3 are carefully adjusted, to ensure

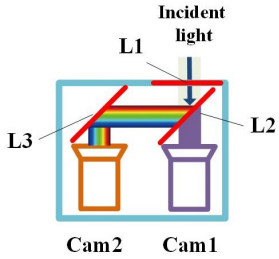

FIG. 1. Schematic of the corona-discharge detection system.

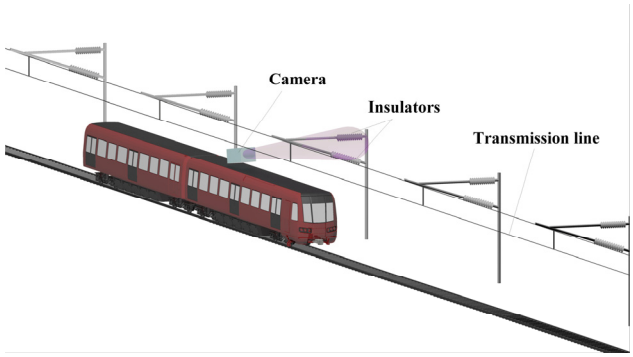

FIG. 2. Experimental setup for railway inspection.

that the two cameras observe an identical field of view. Owing to this, the location where UV emission occurs can be precisely positioned by superimposing the UV image upon the visible video image of the surrounding environment.

The detection system was mounted on top of the train during the experiment, as shown in Fig. 2. The system was set at an appropriate angle, to observe both the transmission line and the electrical insulators placed along the railroad. During the experiment, the train ran along the railroad and the bi-spectral camera observed all the apparatus along the way.

III. ALGORITHM

3.1. Characteristics of the UV Targets

The detection of weak UV radiation is achieved by the ICCD mentioned above. The ICCD was operated at sufficiently high gain such that a single incident photon impinging on the photocathode could be converted to a large number of electrons finally arriving at the phosphor inside the ICCD, resulting in a bright spot on the final grayscale image [14, 15]. Extremely weak UV radiation could be detected through the intensification of the ICCD. However, in the meantime some noise signals, such as the dark current of the detector and leakage photons from the environment that were not completely filtered, are also intensified by the image intensifier, resulting in bright spots on the acquired image that are similar to those generated by the UV radiation to be detected. A typical grayscale image acquired at a high gain level is shown in

Fig. 3. The bright spots inside the yellow block are from the emitter, while other spots are noise interruptions. The spots generated by the emitted UV radiation and noise could not be well distinguished by grayscale level or size.

Most of the time the train runs along a straight railway, whereas the target is located at a fixed position. Taking the train as a reference, the target moves linearly. The trajectory of the target's image in the camera is also a line, after a simple projective transformation. Therefore, it is possible to distinguish the targets from background noise among the bright spots in the image by observing the movement track of each spot between frames. A target would move along a line in a series of consecutive frames, while the other spots might appear at irregular positions.

Moreover, the movement tracks of the target on the detector can be calculated beforehand, which is beneficial for reducing the computational complexity and the false-alarm rate of the algorithm. The movement tracks are calculated as follows:

The focal length of the UV camera lens is f. Let (x_0, y_0, z_0) be the coordinates of a point P in the object space, and (x, y, f) the coordinates of the image point P' in the image plane. A projective relationship between the two points is mathematically expressed by the form

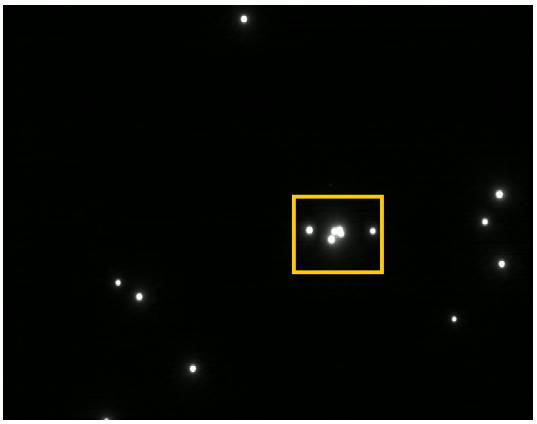

FIG. 3. A frame of grayscale image acquired by the UV camera, showing both signal and noise.

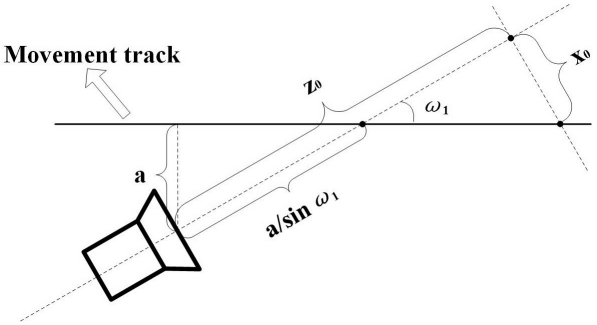

FIG. 4. Projection onto the x-z plane of the relationship between a movement track and the camera.

$$\frac{x_0}{z_0}=\frac{x}{f}$$
$$\frac{y_0}{z_0}=\frac{y}{f}\ . \tag{1}$$

For points along the movement track (straight line) of the target, the values of x_0 and y_0 both depend on the value of z_0. The value of x_0 is considered first. For easier deduction, the movement track and camera are projected onto the x-z plane, as shown in Fig. 4. The distance between the camera and movement track on the x-z plane is a. The angle between the trajectory of the target and the optical axis of the camera is ω_1. The values of a and ω_1 are known before the experiment. The values of x_0, z_0, and ω_1 do not vary during the projection. After a simple deduction, the relationship between x_0 and z_0 is expressed as follows:

$$x_0=(z_0-a\sin\omega_1)\tan\omega_1 \tag{2}$$

After a similar deduction, the relationship between y_0 and z_0 is given as

$$y_0=(z_0-b\sin\omega_2)\tan\omega_2 \tag{3}$$

Solving Eqs. (1), (2), and (3) for x and y, we obtain

$$y=\frac{b\cos\omega_1}{c\cos\omega_2}x+f\frac{a\sin\omega_2-b\sin\omega_1}{a\cos\omega_2} \tag{4}$$

Eq. (4) illustrates the movement track of the target on the UV detector, which is a line with slope and intercept determined by the angle and distance between detector and target.

3.2. Preprocessing of the Grayscale Image Acquired by the UV Camera

Preprocessing of the grayscale image acquired by the UV camera is necessary to use the Hough transform. As discussed above, the grayscale data and sizes of the bright spots are not helpful in distinguishing weak emission from background noise. Only the locations of the bright spots on each frame are interesting. Therefore, as the first step of preprocessing, the centroids of the bright spots in the original grayscale image need to be calculated.

3.3. Algorithm Based on Hough Transform for Target Recognition

As discussed in Section 3.1, the targets could be distinguished from background noise among the bright spots by observing the movement track of each spot between frames. For a single frame, the motion of each bright spot could be obtained by analyzing its centroid in the present frame and in previous frames. The linear

motion of a spot can be tracked with a simple algorithm based on Hough transform [9]. The spots with linear trajectories in the present frame are then labeled as suspected corona discharge.

The Hough transform voting scheme is an effective algorithm to identify the supporting lines of sets of collinear pixels in images. In Duda and Hart's approach [10], pixels are mapped to lines in a discretized two-dimensional parameter space with an angle-radius parametrization based on the equation

$$x\cos(\theta)+y\sin(\theta)=\rho, \tag{2}$$

where x and y are the coordinates of the pixel in the image, ρ is the distance from the origin of the image's coordinate system to the line, and θ is the angle between the image's x-axis and the normal to the line. The cells of the parameter space with the largest amount of votes represent the lines best fitting the collinear pixels.

A slight modification is made in the above voting scheme to achieve the recognition of corona targets: The coordinates of the centroid of each spot in the present frame and several previous frames are mapped to the parameter space. Then the numbers of votes for each cell are counted. Cells with numbers of votes above a threshold represent the linear tracks detected in the present frame of the image. The number of previous frames involved in the calculation is determined by the number of frames in which an object would appear in the view of the camera during the cruise, which is further determined by several practical factors such as the speed of the train, the distances between objects and camera, the field of view of the camera. In our experiment that will be demonstrated in the next section, the objects we were observing would appear in about ten consecutive frames of image acquired by the camera. Therefore nine previous frames were involved in the calculation. The threshold for line judging is also determined by practical factors.

The UV camera's field of view is very narrow, to achieve high sensitivity. During high-speed running, an object would appear in only about ten frames of picture. To achieve high probability of detection, an 8-of-12 detector was designed for the Hough-transform-based algorithm. Under the original algorithm for an 8-of-12 detector, eight spots appearing along a line would be confirmed as a target. However, in situations with high noise levels it is possibly that eight interrupting spots might appear along a straight line. In such cases, false alarms would arise.

To limit the probability of a false alarm to acceptable levels, modifications to the standard Hough transform voting scheme were applied in our algorithm. The first modification is to limit the ranges of θ and ρ by predicting them according to Eq. 8, which is a method in the spatial domain. The time cost and false-alarm rate of the algorithm could be improved by introducing this limitation.

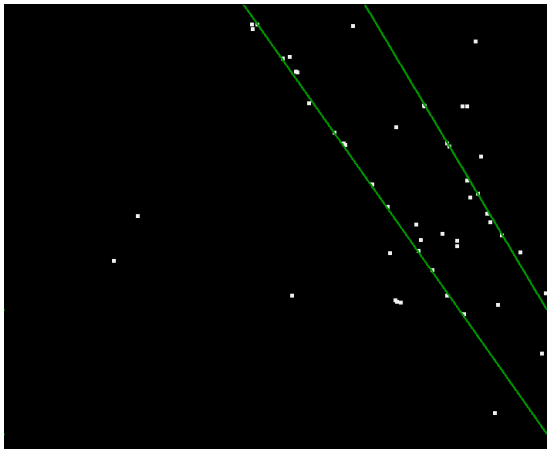

FIG. 5. Example of linear-movement-track detection with our algorithm.

In addition, the targets move along the detected straight lines only in a particular direction. To further decrease the false-alarm rate, detected lines that do not conform to this characteristic, which might be due to noise, must be neglected. This method is similar to adding a third, temporal dimension to the Hough transform. Compared to a three-dimensional Hough transform, however, our algorithm is simpler and costs less time. Limitations in the spatial and temporal domains are especially significant when the noise level is relatively high.

An example of linear-movement-track detection based on this algorithm is shown in Fig. 5. In this binary image, the grayscale values of pixels pointing to the centroids of spots in ten consecutive frames are set to be 255, while the grayscale values of other pixels are set to zero. Two lines are detected using the modified Hough transform voting scheme. These two lines present two linear tracks, indicating that two targets are detected in the present frame of the image.

IV. EXPERIMENTS AND DISCUSSION

4.1. The Arrangement of the Experiment

The experiment was carried out during a routine inspection of railways in Xinjiang Province, China. Our corona camera (Fig. 6) was mounted on top of the train, as shown in Fig. 7. A computer was placed inside the train. Camera control and target recognition were realized by a program written in the C language.

4.2. Results and Discussion

Figure 8 shows an example of an emitting object tracked by the system. The grayscale image of UV channel is overlaid on the visible image, after being transformed to a binary image by applying a proper threshold. The red spots on the images are the bright spots in the UV image.

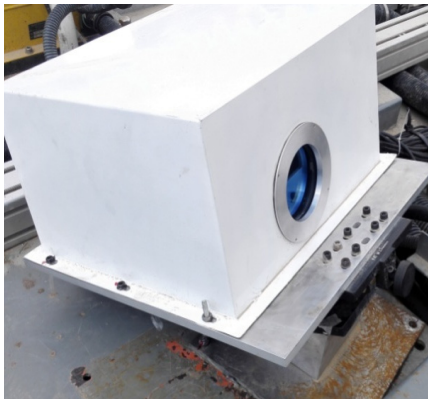

FIG. 6. Photograph of the bi-spectral camera used for corona detection.

FIG. 7. Photograph of the experiment setup.

(a) Frame 2915

(b) Frame 2917

(c) Frame 2919

(d) Frame 2921

(e) Frame 2923

FIG. 8. An example of UV emission tracked by the detection system.

In the presence of noise interruptions, a number of UV emitters (corona discharges) along the railway were tracked during cruising. A UV emitter on the surface of an electrical transmission line was recognized, as shown in Fig. 8. The UV emitter was blocked by the pantograph of the train in Fig. 8(d), so no target was detected in that frame of the image. The discharge might arise from a defect on the surface of the transmission line. The discharge in this location could result in wasted energy, and indicated a potential failure of the apparatus, which needed a more in-depth examination by professional staff.

The time cost of the algorithm on our computer is approximately 6 ms for each frame of image, enabling real-time recognition of target emitters. The false-alarm rate was under one time per hour during this experiment, which is acceptable in the inspection works.

4.3. False-alarm Evaluation

To further evaluate the performance of our algorithm, a simulated experiment was carried out to calculate the false-alarm rate of the detection algorithm. As discussed in Section 3.3, false alarms arise from interrupting bright spots in the captured picture, which might be due to the dark current of the UV detector or photon leakage from

TABLE 1. False-alarm rates for different noise levels

Number of noise spots (/frame)	False alarm of our algorithm (times per hour)	False alarm of standard hough transform algorithm (times per hour)
1	0	0
2	0	0
3	0	0
4	1	3
5	2	19
6	14	84
7	37	233
8	107	619
9	241	1297
10	511	2254

the surroundings. The practical performance of the algorithm could be judged by its capability of working against these noise interruptions.

The results of the simulation concerning the false-alarm rate of the algorithm is shown in Table 1. The false alarms at different noise levels, illustrated by the average number of interrupting spots in each frame of the picture, were calculated by generating random bright spots in each frame of the UV picture. The false-alarm rates for our algorithm and the standard Hough transform algorithm are both listed in the table. Our algorithm proved to show better performance under noise interruptions, owing to its limitation methods in the spatial and temporal domains.

It was also found in the simulation that the performance of the algorithm exhibits an acceptable false-alarm rate (under two incidents per hour) in situations where there were fewer than five noise spots per frame of picture. When the noise level went higher, the false-alarm rate rose rapidly, which could spoil the accurate recognition of corona discharges. Usually the noise level of our UV detection system was around three or four interrupting spots per frame, so the algorithm in this paper is capable of maintaining a relatively low probability of false alarms in practical inspections.

V. CONCLUSION

An automatic railway corona-discharge detection system based on solar-blind ultraviolet detection was presented in this work. This system can be utilized in both daytime and nighttime, because the solar-blind UV camera does not respond to solar irradiation. Real-time recognition of the radiation emitted from weak corona discharge is realized by an algorithm based on the Hough transform, as proposed in this work. The algorithm proposed in this Letter could be also utilized in other applications, such as unmanned airborne or vehicle-borne UV corona-discharge detectors.

ACKNOWLEDGMENT

This research was supported by a grant from the National High Technology Research and Development Program of China (863 Program) (No. 2015AA033201).

REFERENCES

1. V. M. Moreno and R. S. Gorur, "Effect of long-term corona on non-ceramic outdoor insulator housing materials," IEEE Transactions on Dielectrics and Electrical Insulation **8(1)**, 117-128 (2001).
2. A. J. Phillips, D. J. Childs, and H. M. Schneider, "Aging of nonceramic insulators due to corona from water drops," IEEE Transactions on Power Delivery **14(3)**, 1081-1089 (1999).
3. B. Pinnangudi, R. S. Gorur, and A. J. Kroese, "Quantification of corona discharges on nonceramic insulators," IEEE Transactions on Dielectrics and Electrical Insulation **12(3)**, 513-523 (2005).
4. M. Lindner, S. Elstein, P. Lindner, J. M. Topaz, and A. J. Phillips, "Daylight corona discharge imager," High Voltage Engineering, 1999. Eleventh International Symposium on (Conf. Publ. No. 467) **344**, 349-352 (1999).
5. M. B. Lindner, S. Elstein, and P. Lindner, "Solar blind and bispectral imaging with ICCD, BCCD, and EBCCD cameras," Spies International Symposium on Optical Science **3434**, 22-31 (1998).
6. EPRI, "Guide to corona and arcing inspection of substations," (2002).
7. EPRI, "Guide to corona and arcing inspection of overhead transmission lines," (2002).
8. X. Li, C. Zhu, X. Zhu, Z. Xu, X. Zhuang, X. Ji, and F. Yan, "Background limited ultraviolet photodetectors of solar-blind ultraviolet detection," Applied Physics Letters **103(17)**, 171110 (2013).
9. H. P. V. C, "Method and means for recognizing complex patterns," Google Patents (1962).
10. R. O. Duda and P. E. Hart, "Use of the hough transformation

to detect lines and curves in pictures," Commun. ACM **15(1)**, 11-15 (1972).
11. B. D. Carlson, E. D. Evans, and S. L. Wilson, "Search radar detection and track with the Hough transform. III. Detection performance with binary integration," IEEE Transactions on Aerospace and Electronic Systems **30(1)**, 116-125 (1994).
12. Yankowich and Steve W., "Hough transform based multisensor, multitarget, track initiation technique," Optical Engineering **37(7)**, 2064-2077 (1998).
13. L. R. Moyer, J. Spak, and P. Lamanna, "A Multi-dimensional hough transform-based track-before-detect technique for detecting weak targets in strong clutter backgrounds," IEEE Transactions on Aerospace and Electronic Systems **47(4)**, 3062-3068 (2011)
14. B. R. Sandel and A. L. Broadfoot, "Statistical performance of the intensified charged coupled device," Appl. Opt. **25 (22)**, 4135-4140 (1986).
15. M. A. Sartor, "Characterization and modeling of microchannel plate intensified charge coupled device signal to noise ratio variations with image size," The University of Arizona (1992).